Liquid Crystals
Publication details, including instructions for authors and subscription information:
http://www.informaworld.com/smpp/title~content=t713926090

Elastic, dielectric and optical constants of the nematic mixture E49

S. Faetti[a]; B. Cocciaro[b]
[a] Polylab of INFM and Dipartimento di Fisica, Università di Pisa, Largo Pontecorvo 3, Pisa, Italy [b] Liceo Scientifico XXV Aprile, via Milano 2, Pontedera, Italy

To cite this Article Faetti, S. and Cocciaro, B.(2009) 'Elastic, dielectric and optical constants of the nematic mixture E49', Liquid Crystals, 36: 2, 147 — 156
To link to this Article: DOI: 10.1080/02678290902736903
URL: http://dx.doi.org/10.1080/02678290902736903

Liquid Crystals,
Vol. 36, No. 2, February 2009, 147–156

Taylor & Francis
Taylor & Francis Group

Elastic, dielectric and optical constants of the nematic mixture E49

S. Faetti[a]* and B. Cocciaro[b]

[a]*Polylab of INFM and Dipartimento di Fisica, Universita` di Pisa, Largo Pontecorvo 3, 56127 Pisa, Italy;* [b]*Liceo Scientifico XXV Aprile, via Milano 2, 56125 Pontedera, Italy*

(Received 16 January 2007; final form 8 February 2008)

The Merck nematic mixture E49 exhibits a large nematic interval (0–100 °C) and a large dielectric anisotropy. Both of these features make E49 interesting for applications and basic physics. Unfortunately, no systematic measurements of the material constants of this mixture and their temperature dependence have been reported in the literature. In this paper we report experimental measurements of the splay and bend elastic constants (K_{11} and K_{33}) of the ordinary and the extraordinary refractive indices (n_{ort} and n_{par}) at the wavelength $\lambda = 632.8$ nm and of the two elastic constants parallel and orthogonal to the director (ϵ_{par} and ϵ_{ort}) at the frequency $\nu = 5$ kHz. The temperature dependence of all of these parameters is found in the temperature range 25–99 °C. The measurements of the elastic constants are performed using both a dielectric and an optical method simultaneously on the same nematic sample. The results obtained using the two methods are in a satisfactory agreement between them within the estimated experimental uncertainty. The ordinary and the extraordinary indices are measured using the prism method.

Keywords: liquid crystals; elastic constants; dielectric constants

1. Introduction

Nematic liquid crystals (NLCs) (*1*) have been the object of a lot of attention both for their relevance to basic physics and for the applications in the optoelectronic industry. In both cases, a NLC with a large temperature interval of existence of the anisotropic nematic phase and a large dielectric anisotropy is often required. Both of these conditions are satisfied by some nematic mixtures of cyanobiphenyls as well as the Merck nematic mixture E49. According to the producer datasheet, this material presents a nematic interval ranging from 0 to 100 °C and a relative dielectric anisotropy $\Delta\epsilon = 16.6$ at room temperature ($T = 20$ °C) and at the frequency $\nu = 1$ kHz. Unfortunately, to the best of the authors' knowledge, no systematic measurements of the material parameters of this mixture have been reported in the literature. In this paper, we report experimental measurements of the splay and bend elastic constants (K_{11} and K_{33}), of the ordinary and the extraordinary refractive indices (n_{ort} and n_{par}) and of the dielectric constants parallel and orthogonal to the director (*1*) (ϵ_{par} and ϵ_{ort}) at the frequency $\nu = 5$ kHz. Two different methods to measure the elastic constants are used with a single experimental apparatus. The simultaneous use of two different methods allows us to check the reliability of the experimental results directly. The temperature dependence of all of these material parameters is found in the temperature range 25–99 °C.

The experimental methods to measure the elastic constants are based on the measurement of the distortion of the average molecular axis (director **n**) induced by an electric field (*1*). The director distortion is detected by measuring both the capacitance of the plane capacitor filled with the NLC and the optical dephasing of a transmitted monochromatic beam. The presence of a finite pretilt angle θ_p of the director at the interfaces and of a finite zenithal anchoring energy (*2, 3*) is taken into account. The experimental results obtained with the two methods for the splay elastic constant K_{11}, the bend elastic constant K_{33} and the surface tilt angle θ_p are in a satisfactory agreement between them. The analysis of the capacitance measurements also provides the dielectric constants ϵ_{par} and ϵ_{ort} along the directions parallel and orthogonal to the director, respectively (*1*). The optical method also provides the anisotropy of refractive indices $\Delta n = n_{par} - n_{ort}$. The separate values of the extraordinary and ordinary refractive indices n_{par} and n_{ort} are measured with a different experimental apparatus using the prism method (*4, 5*) in a reflected light configuration. The refractive index anisotropy $\Delta n = n_{par} - n_{ort}$ obtained by the prism method measurements is in a satisfactory agreement with that obtained from the measurements of the optical dephasing.

*Corresponding author. Email: faetti@df.unipi.it

ISSN 0267-8292 print/ISSN 1366-5855 online

DOI: 10.1080/02678290902736903
http://www.informaworld.com

2. Experimental methods

2.1 Measurements of elastic and dielectric constants

The experimental method is a standard method based on the measurement of the response of the NLC to an external field (*6–9*). The NLC is sandwiched between two parallel plates covered by thin ITO (indium thin oxide) conducting layers and maintained at a distance $d \approx 25$ μm by two spacers. A thin rubbed polyimide layer (thickness lower than 0.1 μm) is deposed on the two plates to induce a planar director orientation with a small pretilt angle θ_p on both of the surfaces. An ac voltage at the frequency of 5 kHz is applied between the two ITO conducting layers to generate an electric field **E** along the z-axis orthogonal to the plates. The period of the oscillating field is much smaller than both the director reorientation time and the relaxation time of ionic charges. Under these conditions, the director field does not follow the electric field oscillations but is only sensitive to the constant root mean square (rms) value of the electric field. Furthermore, no space charge is present in the nematic layer that behaves as an ideal dielectric medium (the electric displacement D is constant). The dielectric field at a given distance z from one surface is $\mathbf{n} = [\cos\theta(\mathbf{z}), \mathbf{0}, \sin\theta(\mathbf{z})]$, where $\theta(z)$ is the angle between the director and the surface plane. The equilibrium value of function $\theta(z)$ can be obtained minimising the total free energy of the NLC layer per unit surface area (*1*):

$$F = \int_0^d (F_{el} + F_E)\, dz + W(\theta_1) + W(\theta_2), \qquad (1)$$

where

$$F_{el} = \frac{1}{2}(K_{11}\cos^2\theta + K_{33}\sin^2\theta)\left(\frac{d\theta}{dz}\right)^2 \qquad (2)$$

is the elastic free energy density,

$$F_E = \frac{D^2}{2\epsilon_0(\epsilon_{ort}\cos^2\theta + \epsilon_{par}\sin^2\theta)} \qquad (3)$$

is the dielectric free energy density and

$$W(\theta_i) = \frac{W_0}{2}\sin^2(\theta_i - \theta_p) \qquad (4)$$

is the zenithal anchoring energy (*2*, *3*) with $i = 1, 2$ corresponding to the two plane surfaces of the nematic layer. Here θ_1 and θ_2 are the values of the zenithal director angles at surfaces $z = 0$ and $z = d$, respectively, D is the electric displacement which is constant because no space charge is present and W_0 is the zenithal anchoring energy coefficient that measures the strength of the aligning torques at the surfaces.

To obtain the theoretical value of $\theta(z)$ we follow here the numerical procedure proposed by Stallinga *et al.* (*6*). The minimisation of the total free energy using this approach leads to a system of three integral equations that are solved by a numerical iterative procedure with a relative accuracy better than 10^{-9}. Once the function $\theta(z)$ has been obtained, the nematic capacitance C_N and the optical dephasing $\Delta\phi$ can be easily calculated for each value of the rms value V_0 of the applied voltage. Here $C_N(V_0)$ and $\Delta\phi(V_0)$ depend on the material bulk and surface parameters of the NLC, then these latter parameters can be obtained from the best fit of the experimental values of $C(V_0)$ and $\Delta\phi(V_0)$ to the theoretical curves. As shown in previous papers (*7–9*) the different portions of the curves are differently sensitive to the various unknown parameters. This makes it possible to obtain the best fit values of the unknown material parameters of the NLC with a satisfactory accuracy. For instance, the dielectric constants ϵ_{ort} and ϵ_{par} can be obtained directly from the analysis of the capacitance curve $C_N(V_0)$ in the region of small applied electric fields (below the Freederickz threshold (*1*)) and in the high electric field region, respectively. Furthermore, the anchoring energy coefficient can be easily obtained using the Yokoyama–van Sprang method (*3*) looking at the high fields behaviours of $\Delta\phi(V_0)$ and $C_N(V_0)$. For our strongly rubbed polyimide layers, the anchoring energy coefficient is found to be strong (*2, 3*) and the extrapolation length $L_{ext} = K_{11}/W_0$ is smaller than 0.05 μm at any temperature. This value is much smaller than the thickness $d \approx 25$ μm of the NLC and, thus, for the analysis of the experimental results, we can always assume strong anchoring (*2, 3*). For more details on the fitting procedures, we refer the reader to (*7*). In principle, the presence of the two thin polyimide layers could give a contribution to the measured capacitance. However, owing to the relatively high thickness of the nematic layer ($\approx$25 μm) as compared with the thickness of the polymeric layers ($<$0.1 μm), the effect of the polyimide on the capacitance can be disregarded in the present experiment (its contribution is always smaller than 1%).

The experimental apparatus for the simultaneous measurements of the electrical capacitance and the optical dephasing of the NLC is shown schematically in Figure 1. A diode laser beam of wavelength $\lambda = 637.5$ nm is polarised by polariser P, is focused by the optical lens L_1 at normal incidence on the central region of the cell, passes through the crossed analyser A and is focused by the optical lens L_2 on photodiode Ph. The diameter of the laser spot on the nematic layer is approximately 0.2 mm. The photodiode output is sent to the current amplifier CA and to the low pass filter FI with 1 Hz cutoff frequency.

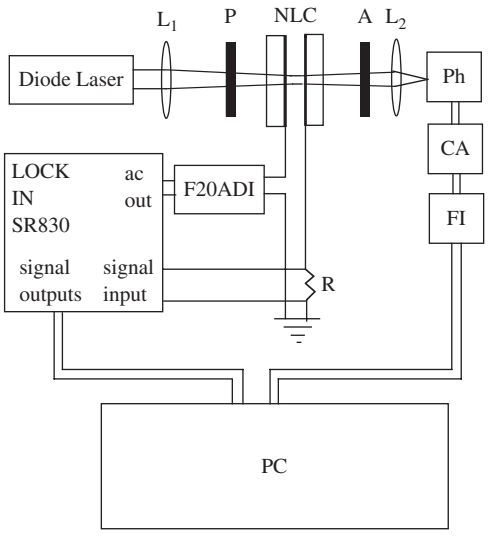

Figure 1. Schematic draft of the experimental apparatus for simultaneous dielectric and optical measurements: *P*, polariser; L_1, optical lens; *A*, analyser; L_2, optical lens; *Ph*, photodiode; *CA*, current amplifier; *FI*, low pass filter; NLC, cell containing the NLC; *PC*, personal computer with an analog–digital interface; F20ADI, high-voltage amplifier; *R*, (=10 Ω) resistance.

The drift of the laser beam intensity is lower than 0.1% per hour. The photodiode output signal I_{Ph} of the photodiode is proportional to the intensity I of the transmitted beam. The angle between the polariser axis and the director is set at 45°. An ac electric voltage at frequency ν = 5 kHz, generated by the Stanford lock-in amplifier SR830, is amplified by the high-voltage F20ADI amplifier and sent to the nematic cell in series with a resistance R = 10 Ω. The voltage drop V_R on resistance R, that is proportional to the electric current flowing in the nematic layer, is sent at the input of the lock-in amplifier that measures the rms values $V_R(0°)$ and $V_R(90°)$ of the in-phase component and of the quadrature component, respectively.

The nematic cell is enclosed in a thermostatic box (Instec HS1) that ensures a temperature accuracy and uniformity better than 0.1 °C. The experiment is entirely controlled by a PC through a 16-bit National Instruments analog–digital interface using the Labview program. The Labview program set a temperature value of the cell and changes, by successive voltage steps, the applied voltage rms in the range 0.6–25 V rms (the Freederickz threshold voltage is close to 0.9 V). In the voltage range close to the Freederickz transition, the reorientation time of the NLC increases greatly (*1*) (slowing down). Then, for any voltage change, the acquisition of $V_R(0°)$, $V_R(90°)$, I_{Ph} and of the rms value of the applied voltage V_0 occurs after a 120 s delay. In order to reduce the total measuring time without losing important details of the response curves $C(V_0)$ and $\Delta\phi(V_0)$, the amplitude of the voltage steps provided by the Labview program is not constant but is appreciably smaller in the voltage range 0.6–1.6 V close to the Freederickz threshold. With these choices, the total measuring time at a given temperature T is about 3 hours. Once a voltage sweep is terminated, the temperature of the nematic cell is changed by the PC and, after a relaxation time of 10 min, a new voltage sweep starts. A complete set of measurements needs about 40 hours time.

In order to avoid dielectric changes due to contamination of the NLC by impurities (*10*), the measurements are performed on a fresh nematic sample and the total measuring time is much smaller than the typical degradation time (several weeks). At a frequency of ν = 5 kHz, the Ohmic resistance and the dielectric losses of the ITO layers are completely negligible as well as the inductance of wires. Then the nematic cell is well represented by a capacitor of total capacitance C_{tot} in parallel to a resistor of resistance R_{N} (the R = 10 Ω resistance in series to the cell is completely negligible here). At any acquisition, the Labview program calculates the total capacitance C_{tot} and resistance R_{N} of the cell using the measured values of $V_R(0°)$ and $V_R(90°)$. The measured total capacitance is the sum of a spurious contribution C_s due to external wires in the circuit and the true capacitance $C(V_0) = \epsilon(V_0)C_0$ of the nematic layer, where $\epsilon(V_0)$ is the effective dielectric constant at the voltage V_0 and C_0 is the capacitance of the vacuum plane capacitor. Therefore, the dielectric constant $\epsilon(V_0)$ is calculated by the Labview program using the simple formula

$$\epsilon = \frac{C_{\mathrm{tot}} - C_s}{C_0}. \tag{5}$$

Here, C_0 and C_s are obtained preliminarily by measuring the total capacitance of the vacuum cell ($C_{\mathrm{tot}} = C_s + C_0$) and that of the same cell filled with cyclohexane $C_{\mathrm{tot}} = C_s + \epsilon C_0$ with $\epsilon = 2.010$ at temperature $T = 22°$). Then, the cell is put under vacuum for 5 hours to evaporate the cyclohexane completely. Finally, the NLC E49 is introduced via a capillary into the cell which is observed at the polarising microscope in order to control the homogeneity of the director alignment. The thickness of the vacuum cell at the centre is measured using interferometry and is $d = 24.8 \pm 0.1$ μm. Thickness variations in the whole nematic cell are less than 0.5 μm. Owing to thermal expansion, the central thickness d shows a very small increase (0.36 μm) when the temperature is increased from T = 25 °C to 100 °C. This small change of thickness is taken into account for recalculating the value of C_0 at each temperature using the formula

$C_0(T) = C_0(T_0)d(T_0)/d(T)$, where $d(T_0)$ and $d(T)$ are the thickness values at temperatures T_0 and T, respectively.

In order to obtain the phase difference $\Delta\phi$ between the ordinary and the extraordinary transmitted beams, we use the known relation for the transmitted intensity between crossed polarisers (*11*):

$$I = I_0\left[\sin^2\left(\frac{\Delta\phi}{2}\right)\right]. \tag{6}$$

Then, the optical dephasing $\Delta\phi$ is obtained from the intensity using the inverse relation:

$$\Delta\phi = 2\arcsin\left[\left(\frac{I}{I_0}\right)^{1/2}\right]. \tag{7}$$

According to (6), the minimum value of intensity should be zero and should be reached for $\Delta\phi = 2N\pi$, while a maximum value I_0 should be reached for $\Delta\phi = 2N\pi + \pi$. Owing to the spurious contributions from multiple reflections at the two interfaces, light diffusion and spatial inhomogeneities of thickness and orientation, this theoretical prediction is never completely fulfilled in the experiment and the intensity maxima and minima do not have exactly the same values. The effects due to cell inhomogeneities are appreciably reduced by focusing the laser beam on the cell (diameter spot approximately 0.2 mm). However, differences up to about 4% between maxima are often observed in these experimental conditions as it can be seen in Figure 2 where the typical experimental dependence of $I(V_0)$ is shown.

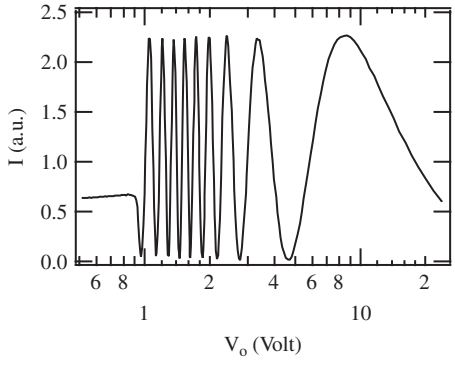

Figure 2. Typical experimental dependence of the transmitted intensity between crossed polarisers (arbitrary unities) on the rms value of voltage applied to the nematic cell. A log scale is used for the horizontal axis to make the curve clearer. Note that maxima and minima have slightly different amplitudes (differences up to 2% are found in this curve). The temperature of the NLC is $T = 35$ °C.

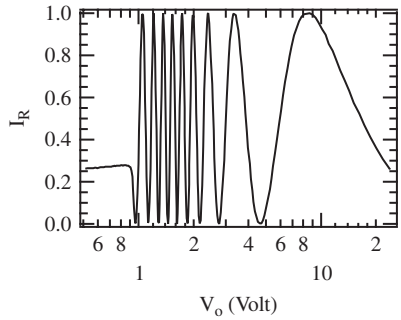

Figure 3. Result of the rescaling of the experimental results shown in Figure 2 using (8).

These spurious contributions can be partially removed by a proper treatment of the experimental data. Using a Fortran program we first approximate the position of all relative maxima and minima of the curve $I(V_0)$, then using a quadratic best fit of the experimental points close to any maxima and minima, we obtain both the best voltage values $V^i_{\min}$ and $V^i_{\max}$ corresponding to maxima and minima and the corresponding intensity values $I^i_{\min}$ and $I^i_{\max}$. Finally, with the Fortran program, we rescale linearly the measured values of $I(V_0)$ in each interval between a minimum and a maximum using the simple relation:

$$I_R = \frac{I - I^i_{\min}}{I^i_{\max} - I^i_{\min}}, \tag{8}$$

where I_R indicates here the renormalised intensity. For simplicity of notation, in the following we still

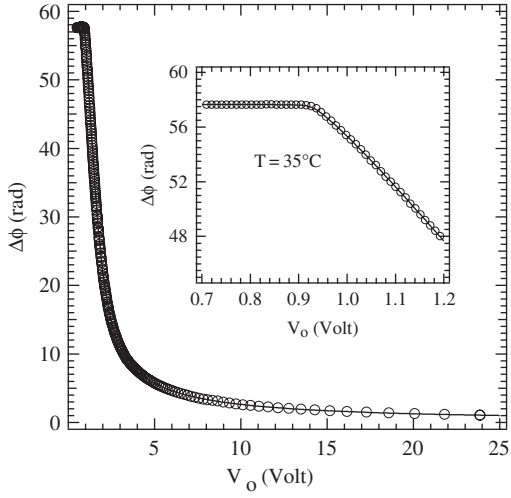

Figure 4. Optical dephasing of the nematic cell versus the rms value of the applied voltage at a temperature $T = 35°$. The full line corresponds to the theoretical best fit with the theoretical solution of equilibrium equations for the director field. The detail of the experimental results close to the Freederickz threshold is shown in the insert.

use the symbol I to indicate the renormalised intensity I_R. With the use of (8) all minima have a zero value while all maxima have an unitary value. The result of this treatment of the experimental results of Figure 1 is shown in Figure 2.

Once the experimental data have been rescaled using the above procedure, the values of the optical dephasing at any voltage are obtained using (7) with $I_0 = 1$. A typical result of this procedure is shown in Figure 4.

2.2 *Measurements of refractive indices*

The experimental apparatus described above for the measurement of the optical dephasing is only sensitive to the anisotropy of refractive indices $\Delta n = n_{par} - n_{ort}$. Therefore, to obtain the separate values of the ordinary and extraordinary refractive indices, a prism method in reflected light has been used. The corresponding experimental apparatus is schematically shown in Figure 5.

The NLC lies between two plane glass plates (1 mm thickness) making a wedge angle $\beta \approx 5°$. A thin (20 nm) SiO layer has been evaporated at 60° (see (*12*)) on the surfaces of the glass plates in order to induce a homogeneous alignment of the NLC. The homogeneity of the alignment is controlled at the polarising microscope. The nematic cell lies inside a thermostatic box ensuring a temperature stability and accuracy better than ±0.1 °C. A monochromatic laser beam (He–Ne, λ = 632.8 nm) passes through an optical lens L (focal length 60 cm), is reflected at 45° by the beam splitter BS and impinges at normal incidence (<0.02°) on the first glass plate (I in Figure 5). The He–Ne laser is used here in place of the diode laser of Figure 1 due to its much better beam quality. The beam reflected by the first surface of the first glass plate (1 in Figure 5) impinges in point O' on a screen. Point O in Figure 5 represents the point where the extrapolation of the incident beam on surface 1 intersects the screen (see Figure 5). Here $h = 2485 \pm 2$ mm denotes the distance of O from the second surface of the first glass plate (2 in Figure 5). The screen has been oriented in such a way to be perpendicular (within ±0.01°) to the beam that is reflected by the first glass plate of the wedge nematic cell. The position of lens L is set to reach the minimum dimension (≈1 mm) of the beam spots on the screen. The distance $\|OO'\|$ between point O and O' is

$$\|OO'\| = \frac{D \sin[\pi/4 - \arcsin(\pi/4n_v)]}{\cos[\arcsin(\pi/4n_v)]}, \qquad (9)$$

where D = 8 mm and n_v = 1.509 are the thickness and the refractive index of the glass beam splitter BS, respectively. By substituting D = 8 mm and n_v = 1.509 in (9), we obtain $\|OO'\|$ = 2.66 mm. When the wedge cell is empty, the beam reflected by the second glass interface impinges on the screen at a distance L_0 from O. The corresponding angle α with the normal to surface 1 is

$$\alpha = \arctan\left(\frac{L_0}{h}\right). \qquad (10)$$

Note that (10) represents an approximated expression, while a rigorous treatment with geometric optics would lead to the same expression as in (10) but with h that is replaced by a slightly different value h_1. However, according to the following discussion and to the analysis given in Appendix 1, the use of this simplified expression for the reflected light prisms method leads to negligible relative error (<0.004%) in the measurement of the refractive indices of the NLC. Owing to the small thermal dilatations of the wedge cell, the angle α (α = 10.366 ± 0.008° at temperature T = 22 °C) increases by about 1% if temperature is increased up to 100 °C. Then, angle α has been measured for any temperature value used in the experiment before the NLC is injected by capillary into the cell. When the NLC is introduced into the wedge cell, the incident beam is separated into the

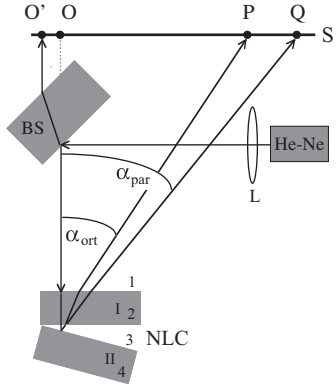

Figure 5. Schematic drawing of the experimental apparatus to measure the ordinary and extraordinary refractive indices. L, optical lens; BS, glass beam splitter. A laser beam impinges at normal incidence on a wedge nematic cell (NLC). The beams reflected by the two plane glass plates of the wedge cell are focused by the optical lens L onto the screen *S*. O' represents the point on the screen where the beam reflected by surface 1 of the first glass plate impinges on the screen. The distance $\|OO'\|$ between points O and O' on the screen is $\|OO'\|$ = 2.66 mm (see (9)). The beams reflected by the second glass plate are separated into an ordinary and an extraordinary beam that impinge on points P and Q on screen S at the distances L_{ort} and L_{par} from point O.

ordinary and the extraordinary rays that are reflected by the second glass plate of the cell and impinge on points P and Q at distances L_{ort} and L_{par} from point O on the screen (see Figure 5). The corresponding deviation angles are

$$\alpha_{ort} = \arctan\left(\frac{L_{ort}}{h}\right) \tag{11}$$

$$\alpha_{par} = \arctan\left(\frac{L_{par}}{h}\right). \tag{12}$$

Here, h should be replaced by two slightly different values h_2 and h_3 in an exact optical treatment (see Appendix 1). The ordinary and extraordinary refractive indices n_{ort} and n_{par} are obtained using the simple formula

$$n_{ort,par} = \frac{\sin(\alpha_{ort,par}/2)}{\sin(\alpha/2)}. \tag{13}$$

The main advantage of using the prism method in a reflected light geometry in place of the standard transmitted light geometry (*4*, *5*) is that the deviation angles α, α_{ort} and α_{par} are obtained by the same experimental apparatus. Then, many systematic sources of error tend to be compensated when (13) is used. For instance, the uncertainty $\Delta h \approx 2$ mm on the measurement of distance h of surface 2 from the screen leads to a relative error of about 0.1% on the measurements of angles α, α_{ort} and α_{par} but a relative error less than 0.003% on the extraordinary and ordinary refractive indices as deduced using (13). This can be easily understood if we note that, for small deviation angles x, $\arctan x \approx x$ and $\sin x \approx x$. Then $\alpha \approx L_0/h$ and $\alpha_{ort,par} \approx L_{ort,par}/h$. Substituting these expressions in (13)), we find $n_{ort,par} \approx L_{ort,par}/L_0$ that is independent of the distance h from the screen. Then, the uncertainty on the h-value affects only the small nonlinear contributions in (13).

Similarly, replacing the exact distances h_1, h_2 and h_3 with h in (10)–(12) leads to a negligible error ($<0.004\%$) on the measured refractive indices (see Appendix 1). With the present reflected light apparatus, the main source of uncertainty is related to the uncertainty $\Delta L \approx 0.2$ mm on the measurement of the position of the centre of the laser spots on the screen (the centre of the laser spot of 1 mm diameter is found using a hand lens). This leads to an error of less than 0.06% on the measured deviation angles α_{ort}, α_{par} and α and, thus, an estimated uncertainty of about 0.1% on the experimental values of the refractive indices. By taking into account that the refractive indices are lower than 1.8, we infer that the absolute uncertainty on the refractive indices measurements is about 0.002.

3. Experimental results

Typical experimental results for the dependences of the optical dephasing $\Delta\phi$ and the dielectric constant ϵ on the rms value of the applied oscillating voltage are shown in Figures 4 and 6, respectively. The temperature of the sample was 35 °C. Details of the behaviour close to the Freederickz threshold voltage ($V_c \approx 0.92$ V) are shown in the insets. Circles in Figure 4 and crosses in Figure 6 represent the experimental results, while the full lines are the best fits with the theory. Note the good agreement between theory and experiment. Similar results are obtained at any temperature. The best fit of the dielectric constant (Figure 6) provides the two dielectric constants ϵ_{ort} and ϵ_{par}, the pretilt angle θ_p and the elastic constants K_{11} and K_{33}. The best fit of the optical measurements (Figure 4) provides the anisotropy Δn of refractive indices, the pretilt angle θ_p and the elastic constants K_{11} and K_{33}. Comparison between the experimental data of θ_p, K_{11} and K_{33} obtained by the two methods gives a direct check of the reliability of the experimental results.

The temperature dependence of the dielectric constants ϵ_{ort} and ϵ_{par} is shown in Figure 7 together with the isotropic constant $\epsilon_{is} = (\epsilon_{par} + 2\epsilon_{ort})/3$. The corresponding temperature dependence of the dielectric anisotropy $\Delta\epsilon = \epsilon_{par} - \epsilon_{ort}$ is shown in Figure 8. The estimated accuracy on the dielectric constants is 1%. In

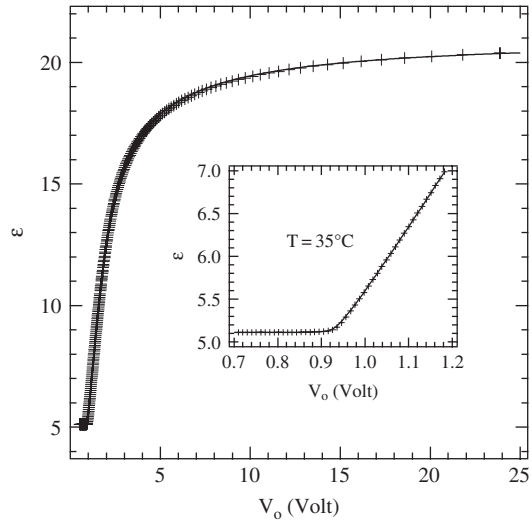

Figure 6. Effective dielectric constant ϵ of the nematic cell versus the rms value of the applied voltage at temperature $T = 35°$. The full line corresponds to the theoretical best fit with the theoretical solution of the equilibrium director equations. The detail of the experimental results close to the Freederickz threshold is shown in the insert.

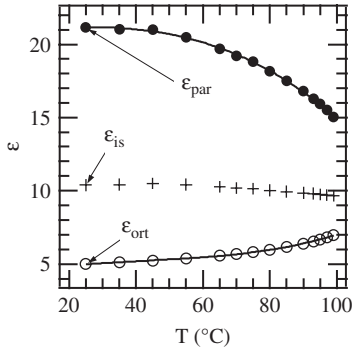

Figure 7. Parallel and orthogonal dielectric constants of the NLC E49 versus temperature T. Here ϵ_{is} represents the isotropic constant $\epsilon_{is} = (\epsilon_{par} + 2\epsilon_{ort})/3$. The full lines represent the best fit with the fourth-order polynomial in (14).

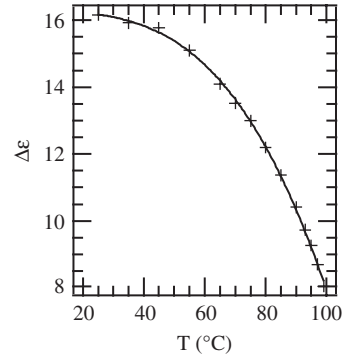

Figure 8. Anisotropy of dielectric constants $\Delta\epsilon = \epsilon_{par} - \epsilon_{ort}$. The full line is the fourth-order polynomial best fit.

order to have a useful analytical formula giving the dielectric constants values at each temperature T in the measurement interval 25–99 °C, we made the best fit of the experimental results with the fourth-order polynomial

$$y = A + BT + CT^2 + DT^3. \qquad (14)$$

The full lines in Figures 7 and 8 represent the best fit curves. The corresponding *A, B, C* and *D* numerical coefficients are given in Table 1. The fitting curves agree with the experimental results within 1%. The values of the dielectric constants reported in the Merck data sheet for E49 at temperature $T = 20°$ and frequency $\nu = 1$ kHz are $\epsilon_{par} = 21.7$ and $\epsilon_{ort} = 5.1$. The small difference (about 3%) with our data at $T = 25°$ is probably due to the different frequency used in the present experiment ($\nu = 5$ kHz) and to the different temperatures.

The temperature dependence of the elastic constants K_{11} and K_{33} is shown in Figure 9. Open circles

Table 1. The coefficients *A, B, C* and *D* of the fourth-order polynomial in (14) that provides the best fit to the temperature dependences of the dielectric constants, of the elastic constants and of the refractive indices.

	A	B	C	D
ϵ_{par}	20.626	0.034298	-4.0831×10^{-4}	-5.0252×10^{-6}
ϵ_{ort}	4.2266	0.046166	-7.9222×10^{-4}	6.0926×10^{-6}
K_{11}	17.680	−0.19505	1.8753×10^{-3}	-1.3722×10^{-5}
K_{33}	27.581	−0.16127	-8.348×10^{-4}	6.5553×10^{-7}
n_{par}	1.821	-1.8868×10^{-3}	2.3166×10^{-5}	-1.8852×10^{-7}
n_{ort}	1.5128	5.6835×10^{-4}	-1.439×10^{-5}	1.1096×10^{-7}

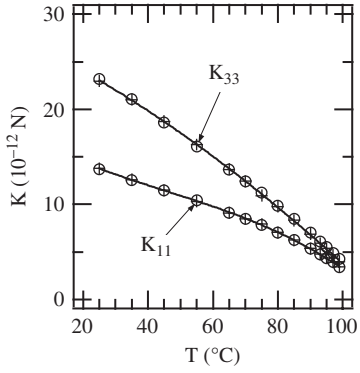

Figure 9. Splay (K_{11}) and bend (K_{33}) elastic constants versus temperature T. Open circles correspond to the optical results while crosses correspond to the dielectric results. The full lines represent the polynomial best fits using (14).

correspond to the results of the optical method while crosses correspond to the results of the dielectric measurements. The full line represents the fourth-order polynomial best fit (see (14)) of the average value of the dielectric and optical elastic constants [$K = (K_{opt} + K_{diel})/2$]. The corresponding best fit coefficients are given in Table 1. The estimated accuracy on the values of the K_{11} elastic constant is better than 2%, while that of K_{33} is 5%. For details on the evaluation of these and other experimental uncertainties we refer the reader to (*7*, *9*).

The relative difference between optical and dielectric measurements of the elastic constants is shown in Figure 10. We see that the K_{11} values obtained by the two methods agree within 1% at each temperature value, while systematic discrepancies up to 4% are observed for K_{33} as far as the high-temperature region is concerned. This latter systematic difference could be related to the fact that the dielectric method measures the average value of the elastic constant in a large region of the cell (1 cm^2), while the optical method measures the average value in the much smaller region where the laser beam is focused ($\approx$0.04 mm^2). Therefore, small spatial variations of the nematic

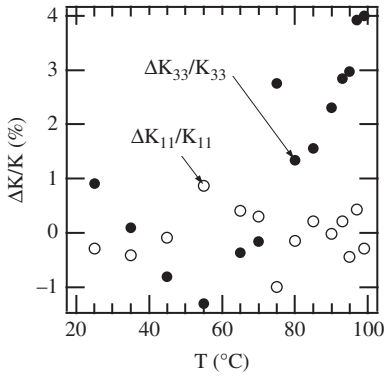

Figure 10. Relative difference $\Delta K/K = [K_{opt} - K_{diel}]/K_{diel}$ between the elastic constants measured with the optical and dielectric methods.

layer thickness or phase separation of different components of the nematic mixture on approaching the transition temperature could be responsible for the observed differences. In fact, in such a mixture the transition to an isotropic phase initiates at a temperature $T \approx 97$ °C with the occurrence of small isotropic regions that grow by increasing the temperature up to cover the entire nematic layer at a temperature of about 104 °C. Therefore, appreciable systematic discrepancies between optical and dielectric measurements are expected to occur at the higher temperatures.

Figure 11 shows the temperature dependence of the surface pretilt angle θ_p as obtained from the optical measurement (open circles) and the dielectric measurements (crosses). We see that the surface angle is about 0.12° and decreases slightly as the temperature is increased. Figure 12 shows the temperature dependence of the anisotropy of the refractive indices. Open circles in Figure 12 represent the anisotropy of the refractive indices as obtained using the optical apparatus of Figure 1. The estimated uncertainty on these measurements (open circles) is expected to be about 1% corresponding to an absolute uncertainty of 0.002 (for details see (*7*)). Crosses in Figure 12 correspond to the results obtained using the prism reflective method. The expected absolute uncertainty of these latter measurements is lower than 0.004 corresponding to a 2% relative uncertainty. The agreement between the two measurements is satisfactory (within 2%), but some systematic difference can be noted. Note that the optical dephasing measurements and the prism method measurements are performed at slightly different optical wavelengths (637.5 and 632.8 nm, respectively). However, the variation of the anisotropy of refractive indices at these two wavelengths is expected to be less than 0.001, which is negligible here (*13*).

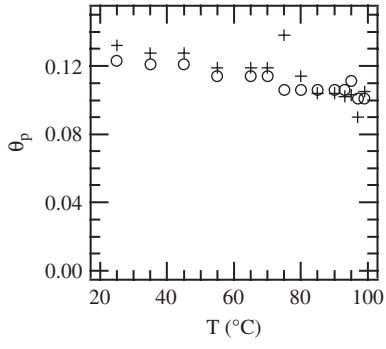

Figure 11. Temperature dependence of the pretilt surface angle θ_p as deduced by optical (open circles) and dielectric (crosses) measurements.

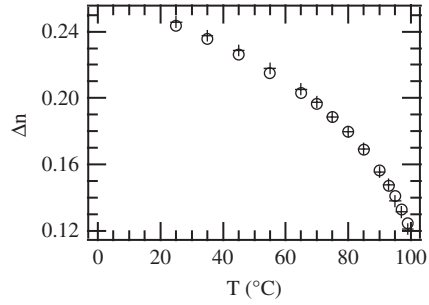

Figure 12. Anisotropy of the refractive indices versus temperature T. Open circles correspond to the result of the measures of optical dephasing, while crosses correspond to the result of the prism method.

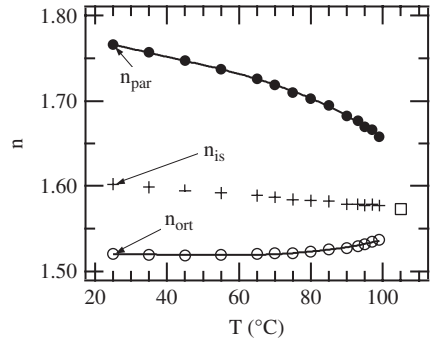

Figure 13. Temperature dependence of the ordinary and extraordinary indices as obtained by the prism method. Here n_{is} is the isotropic refractive index defined as $n_{is} = (2n_{ort} + n_{par})/3$. The open square represents the refractive index that is measured at the temperature $T = 105$ °C where the NLC is in the isotropic phase. The full lines represent the polynomial best fits with (14).

The results of the prism measurements of the ordinary and the extraordinary refractive indices are shown in Figure 13. The estimated accuracy of these

measurements is 0.002. The full lines correspond to the best polynomial fits with the best fit coefficients given in Table 1.

4. Conclusions

In this paper, we have measured the temperature behaviour of the splay and bend elastic constants, of the refractive indices and of the dielectric constants of the nematic mixture E49 using three different experimental methods. This Merck mixture has a large nematic interval (0–100 °C) and a high dielectric anisotropy (≈17). Both of these features make E49 very interesting for applications and for basic physics. The use of different experimental apparatus to obtain the elastic constants provides a direct check of the reliability of the experimental results. A satisfactory agreement between the different sets of experimental data is found within the estimated experimental uncertainties. Fourth-order polynomial fits (see (14)) of the experimental temperature dependence of the material constants are obtained in order to provide a useful analytical formula representing the experimental data in the whole measurement range 25–99 °C. The corresponding best fit coefficients are given in Table 1.

References

(1) de Gennes, P.G.; *The Physics of Liquid Crystals*; Clarendon, Oxford, 1974.
(2) Faetti, S.; *Physics of Liquid Crystalline Materials*; Khoo, I.C. and Simoni, F., Eds.; Gordon and Breach Science Publishers, 1991.
(3) Yokoyama, H.; van Sprang, H.A.; *J. Appl. Phys*. **1985**, *56*, 4520.
(4) Chatelain, M.-P.; Germain, M. *C. R. Acad. Sci*. **1964**, *259*, 127.
(5) Brugioni, S.; Faetti, S.; Meucci, R. *Liq. Cryst*. **2003**, *30*, 927.
(6) Stallinga, S.; van Haaren, J.A.M.M.; van den Eerembeemd, J.M.A.; *Phys. Rev. E* **1996**, *53*, 1701.
(7) Bogi, A.; Faetti, S.; *Liq. Cryst*. **2001**, *28*, 729.
(8) Maze, C.; *Mol. Cryst. Liq. Cryst*. **1978**, *48*, 273.
(9) Bradshaw, M.J.; Raynes, E.P.; Bunning, J.D.; Faber, T.E.; *J. Physique* **1985**, *46*, 1513.
(10) Murakami, S.; Naito, H.; *Jpn. J. Appl. Phys*. **1997**, *36*, 2222.
(11) Bruhat, L.; *Optique*; Masson, Paris, 1965.
(12) Monkade, M.; Boix, M.; Durand, G. *Europhys. Lett*. **1988**, *5*, 697.
(13) Li, J.; Wu, S.T.; Brugioni, S.; Meucci, R.; Faetti, S.; *J. Appl. Phys*. **2005**, *97*, 07305.

Appendix A. Refraction angles in the reflected light method

In this appendix we show that the refractive indices of the NLC can be accurately obtained using the simplified expressions in (10)–(13). Figure A1 shows schematically the geometry of the refracted beams. The incident beam impinges at normal incidence on point H of surface 1 of the glass plate I, impinges on plate II and is reflected at an angle 2β as shown in Figure A1 (β is the wedge angle of the cell). Then, the beam is refracted at the angle γ_i by glass plate I, is refracted at the angle α_i at the glass-air interface and impinges on the screen S at a distance L_i from point O. Here subscript i (i = 1, 2, 3) corresponds to the different cases where the cell is empty (i = 1) or the NLC is inside the cell and the polarisation of the beam is the ordinary polarisation (i = 2) or the extraordinary polarisation (i = 3). Here n_i denotes the refractive index of the material inside the cell, n_v = 1.509 is the refractive index of the glass plate, δ = 200 μm is the average thickness of the cell in the light region, d = 1 mm is the thickness of the glass plate and h = 2485 mm is the distance between point O on the screen and point M on surface 2 of plate I. From Figure A1 we infer

$$\alpha_i = \arctan\left(\frac{L_i}{h_i}\right), \tag{A1}$$

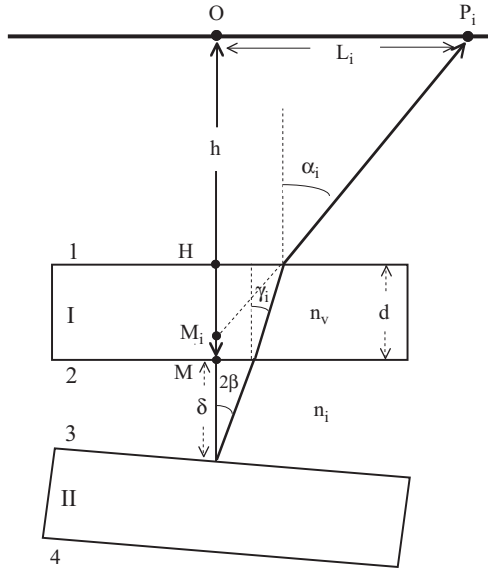

Figure A1. Geometry of the refracted beams in the wedge cell. The incident beam impinges at normal incidence on point H on surface 1 of plate I. The beam reflected by surface 3 of plate II is refracted at angle γ_i at surface 2, then it is refracted at angle α_i at surface 1 and impinges on point P_i on screen S. Here h denotes the distance of the screen from point M on surface 2, L_i denotes the distance of point P_i from point O on the screen and n_i, with i = 1, 2, 3, is the refractive index of the material inside the wedge cell: i = 1 corresponds to the empty cell and i = 2 and i = 3 to the case where the NLC is inside the wedge cell (i = 2 ordinary beam, i = 3 extraordinary beam).

with

$$h_i = h - \|MM_i\|, \tag{A2}$$

where M_i is the extrapolated point shown in Figure A1. The length of the segment $M\ M_i$ in Figure A1 was disregarded in (10)–(12). Here we show that this approximation leads to a negligible error on the measurement of the refractive indices of the NLC. The length $\|M\ M_i\|$ can be easily obtained using the Snell law of refraction for anisotropic media (*11*). In order to make the following analysis clearer, we assume that all of the angles are sufficiently small so that any trigonometric expression can be replaced by its linearised form. Calculations with the full trigonometric expressions lead to the same main conclusion: the length $\|M\ M_i\|$ can be disregarded in (A1)–(A2). According to the Snell law,

$$\gamma_i = \frac{2n_i\beta}{n_v} \tag{A3}$$

and

$$\alpha_i = 2n_i\beta. \tag{A4}$$

Then, with a simple geometrical analysis, we obtain

$$\|MM_i\| = \frac{(n_v - 1)d}{n_v} - \frac{\delta}{n_i}. \tag{A5}$$

The first contribution in the right-hand side in (A5) is $(n_v - 1)d/n_v) \approx d/3 = 0.33$ mm and do not depend on the index i, then it is the same for all of the refracted beams. According to the analysis given in Section 2.2, a constant contribution does not affect appreciably the measurement of the refractive indices. The second term in the right-hand side in (A5) is not constant but depends on index i and, thus, it could affect the measurement of the refractive indices. However, $\delta \approx 0.2$ mm and n_i goes from a minimum value $n_1 = 1$ for the empty cell up to a maximum value $n_3 < 1.8$ for the extraordinary refracted beam. Then, the maximum variation of δ/n_i is $\Delta = \delta/n_1 - \delta/n_3 = 0.09$ mm. This length has to be compared with the distance $h = 2485$ mm. Then, the relative error on the refractive indices that is found using the simplified expressions with $h_i = h$ (see (10)–(13) is expected to be $\Delta/h \approx 0.0036\%$, which is much smaller than the estimated relative uncertainty of our experimental measurements (0.1%). Calculations made using the general trigonometric expressions lead to an analogous estimated uncertainty.